Generation of High-Efficiency Vortex Beam Carrying OAM Mode Based on Miniaturized Element Frequency Selective Surfaces

Yuxiang Wang, Kuang Zhang, Yueyi Yuan, Xumin Ding, Guohui Yang, Jiahui Fu, and Qun Wu

Department of Microwave Engineering, Harbin Institute of Technology, Harbin 150001, China

In this paper, a new method for generating high-efficiency vortex beam carrying orbital angular momentum (OAM) mode is proposed based on the miniaturized element frequency selective surfaces (MEFSS) in the microwave region. The unit cell is a class of sub-wavelength periodic structure, which is composed of non-resonant elements with a low profile. A flat metalens is designed to control the wavefront of the propagating electromagnetic waves based on different phase responses of eight kinds of MEFSS unit cells. Under linearly-polarized normal incidence, a vortex beam carrying OAM mode with a topological charge of 1 is excited. The measurement results are in good agreement with the theoretical prediction and full-wave simulation. The proposed method shows great potential applications in generating OAM mode with high efficiency at microwave frequencies.

***Index Terms*—Metasurface, miniaturized element frequency selective surfaces (MEFSS), orbital angular momentum (OAM).**

I. Introduction

RECENTLY, the vortex beam carrying orbital angular momentum (OAM) has drawn a lot of attention for wireless communication [1], [2]. The generation of OAM mode was first proposed in the optical region [3] and, recently, has been extended to a microwave frequency. Vector antenna arrays were first used to generate OAM beams in radio frequency [4]. Then, the standard antennas arranged in circular arrays were applied to generate a vortex beam [5]. Metasurface was also proposed to be utilized for OAM multiplexed communication [6], and a high-capacity millimeter-wave communication link was realized by transmitting eight multiplexed OAM beams [7]. Due to the orthogonality between different OAM modes, OAM multiplexing is considered as a possible theoretical solution to enhance the capacity of the channel, when the communication system is nearly approaching the Shannon limit [8], [9].

In microwave region, there are several methods to generate OAM modes, including using spiral phase plates [10], antenna array [11], [12], and metasurfaces [13]–[15]. However, most of the currently available technologies have their own limitations in the application at microwave frequency. The thickness of spiral phase plates needs to be varied in an azimuth direction to introduce the phase factor $e^{jl\theta}$, and there could be a sharp increase in thickness and volume as the frequency decreases [16]. The antenna array usually needs a complex feeding network for OAM generation due to the acquired phase difference between array elements [11], which can be a great obstacle when integrated with other equipment. For the metasurface-based phase plate, the design approach of unit cells usually lacks theoretical support; hence, the efficiency and bandwidth of the whole metasurface are usually limited and the relatively low efficiency is the main problem for practical applications [17].

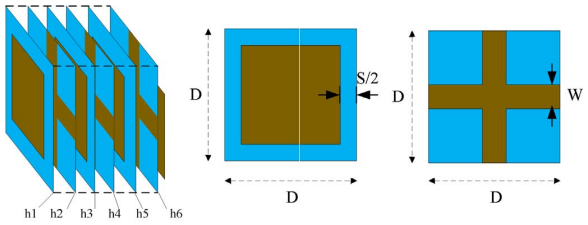

Fig. 1. Fourth-order bandpass MEFSS unit cell.

In this paper, a new method for generating high-efficiency vortex beam carrying OAM mode is proposed based on miniaturized element frequency selective surfaces (MEFSS) in the microwave region. In contrast with the traditional FSS [18], [19], MEFSS is less insensitive to the angle of incidence due to the sub-wavelength dimensions and low overall profile [20]–[22]. A simplified equivalent circuit model for this multilayer structure is established, and a good agreement is observed between the full-wave simulation result and the calculation of the equivalent circuit model. A group of eight unit cells with gradient sizes is proposed with high transmission efficiency in a wide operation band, which is further used to construct the metalens. Both simulations and measurements show that the proposed metalens with a thickness of $0.15\lambda_0$ can generate the OAM mode of $l = 1$, constituting an important result for OAM multiplexing in wireless communication systems.

II. Design of MEFSS Unit Cells

Through cascading multi-layered non-resonant components, a high-order MEFSS is available to exhibit a bandpass response. Fig. 1 shows the 3-D view of MEFSS unit cell, which is composed of four layers of patches and three layers of wire grids alternately separated by dielectric substrates. It is a vertically symmetrical structure that means the top and bottom

Manuscript received November 9, 2018; revised January 26, 2019; accepted May 24, 2019. Corresponding author: K. Zhang (e-mail: zhangkuang@hit.edu.cn).

Color versions of one or more of the figures in this paper are available online at http://ieeexplore.ieee.org.

Digital Object Identifier 10.1109/TMAG.2019.2919715

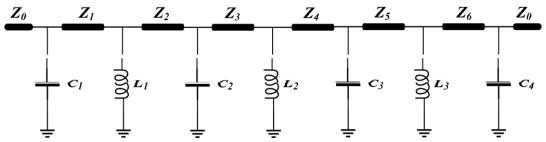

Fig. 2. Simplified equivalent circuit model of the proposed unit cell.

patches, as well as wire grids, have the same dimensions. The period of the unit is D, while the dimensions of metallic patches and metallic grids are P_i and W_i, respectively, the gaps between the adjacent patches are represented by S_i, and h_i is the thickness of the ith layer dielectric substrate. Since the MEFSS structure is symmetric to the center of the unit cell, it is polarization insensitive for normal incidence.

From the point of the equivalent circuit, the unit cell structure can be regarded as a fourth-order bandpass filter. In order to analyze the operating principle of MEFSS as a spatial filter, the equivalent circuit model is established and shown in Fig. 2.

In the circuit model, the metallic patch is equivalent to a capacitor, while the wire grid can be regarded as an inductor, and the dielectric substrates separating them are modeled as transmission lines with the characteristic impedance of Z_i according to the thickness of substrate [23]. Since the unit cells are supposed to work in the free space, the loads are modeled with semi-infinite transmission lines with the characteristic impedance of $Z_0 = 377\Omega$. The effective capacitance value of metallic patches can be described as follows [24]:

$$C_i = \varepsilon_0 \varepsilon_r \frac{2D}{\pi} \ln\left(\frac{1}{\sin\frac{\pi S_i}{2D}}\right) \tag{1}$$

where ε_0 is the permittivity of free space, ε_r is the relative permittivity of the substrate where the patch located, and S_i is the interval between the patches of two adjacent units. Analogously, the inductance value of the wire grids can be approximated using the following formula:

$$L_i = \mu_0 \mu_r \frac{D}{2\pi} \ln\left(\frac{1}{\sin\frac{\pi W_i}{2D}}\right) \tag{2}$$

where μ_0 is the permeability of free space, μ_r is the relative permeability which is usually equal to 1 for the dielectric substrate, and ω_i is the width of the strips. Since the dielectric substrates are modeled with transmission lines, it can be divided into series inductors and shunt capacitors as follows:

$$C_{Ti} = \varepsilon_0 \varepsilon_r h_i \tag{3a}$$

$$L_{Ti} = \mu_0 \mu_r h_i \tag{3b}$$

where L_{Ti} and C_{Ti} represent the equivalent inductance and capacitance of the dielectric substrates.

The dimensions of this MEFSS unit cell are shown in Table I, while the optimized equivalent circuit model parameters are recorded in Table II. The period of MEFSS unit is $D = 6$ mm, nearly approximate to $\lambda_0/5$, where λ_0 is the free-space wavelength at a center operating frequency of 10 GHz, far smaller than the dimension of the traditional FSS unit.

TABLE I
PHYSICAL PARAMETERS OF THE FOURTH-ORDER BANDPASS MEFSS UNIT. ($\varepsilon_r = 3.0$)

Parameter	P_1, P_4	P_2, P_3	W_1, W_3	W_2
Value	5.05 mm	5.70 mm	0.6 mm	1.0 mm
Parameter	h_1, h_6	h_2, h_5	h_3, h_4	D
Value	1.0 mm	0.75 mm	0.5 mm	6.0 mm

TABLE II
EQUIVALENT CIRCUIT VALUES SHOWN IN FIG. 2

Parameter	C_1, C_4	C_2, C_3	L_1, L_3	L_2
Value	126.4 fF	393.62 fF	1542.7 pH	485.5 pH

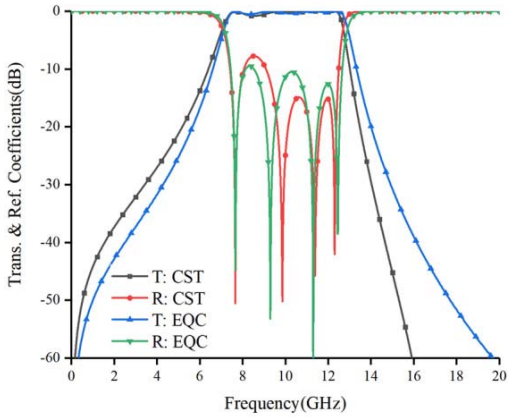

Fig. 3. Calculated and simulated transmission and reflection coefficients of the fourth-order bandpass MEFSS.

Though the MEFSS unit cell owns six layers of the dielectric substrate, the overall thickness is merely 4.5 mm ($0.15\lambda_0$).

Fig. 3 shows the simulated (full-wave simulation by CST Microwave Studio) and calculated (equivalent circuit model by ADS) transmission and reflection coefficients of this fourth-order bandpass MEFSS under the TE- and TM-polarized incidence. As can be seen, a very good agreement between both results is obtained, and the 3 dB transmission bandwidth is about 6 GHz (from 7 to 13 GHz), with a fractional of 60%, in which the phase response can cover a range of 2π.

III. CONSTRUCTION OF METALENS

To generate a vortex beam carrying OAM mode, a group of unit cells with the same phase gradient at center operation frequency is needed. Therefore, eight kinds of MEFSS units with similar structure and gradually changed geometrical size are designed. As shown in Fig. 4(a), the metalens for OAM generation is divided into eight zones with a $\pi/4$ phase shift between adjacent areas and each of them is constructed with the same unit cell. All the unit cells demonstrated in Fig. 4(b) have a high transmission coefficient above 0.9 at 10.6 GHz. The overall phase shift can cover the range of 2π. Then, under the linearly polarized incidence, the transmitted field is expected to be with an additional phase factor mimicking $e^{jl\theta}$ with $l = 1$, and then, a vortex beam carrying OAM with the topological charge of 1 can be excited. If OAM mode with a different mode number is needed, the only factor that needs

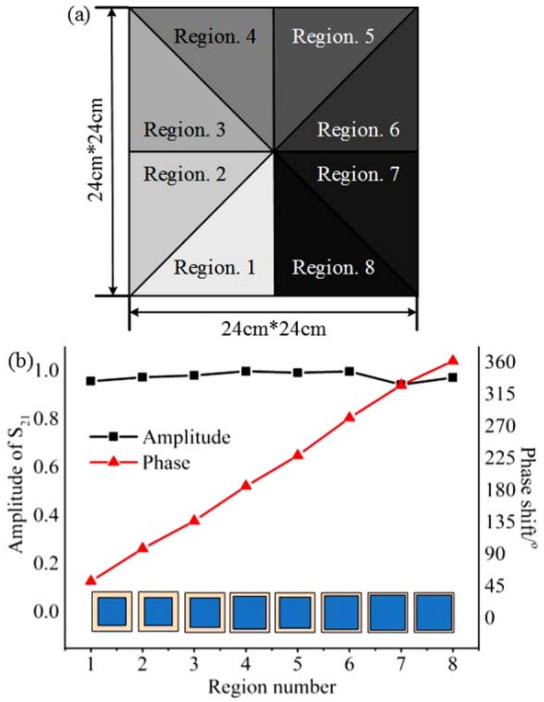

Fig. 4. (a) Division of metalens. (b) Transmission coefficients and phase shift of eight unit cells at 10.6 GHz.

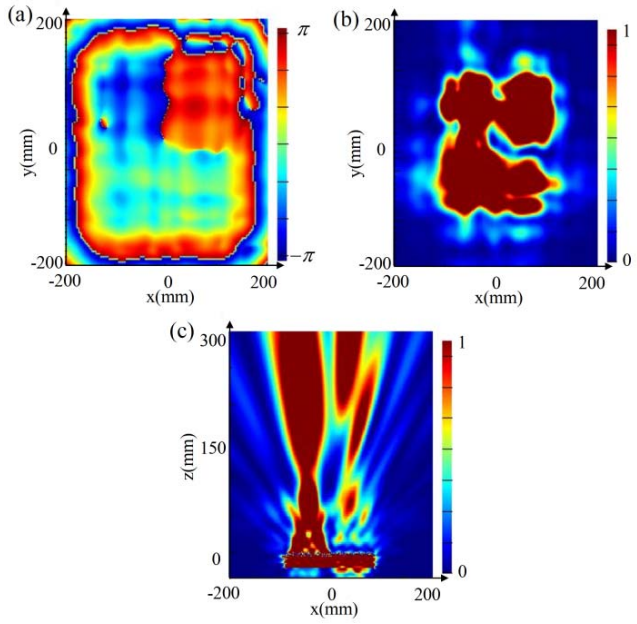

Fig. 5. Simulation result of the near field. (a) Phase distribution at *xoy* plane with $z = 200$ mm. (b) Energy distribution at *xoy* plane with $z = 200$ mm. (c) Energy distribution at *xoz* plane with $y = 0$.

to be adjusted is the phase shift range of the metalens in order to get an integer multiple of 2π based on these MEFSS units.

IV. Simulations and Measurements

The full-wave simulation is conducted by finite-difference time domain (FDTD) solutions to get the phase and intensity distributions. Fig. 5(a) shows the phase distribution of transmitted waves on the *xoy* plane ($z = 200$ mm), and

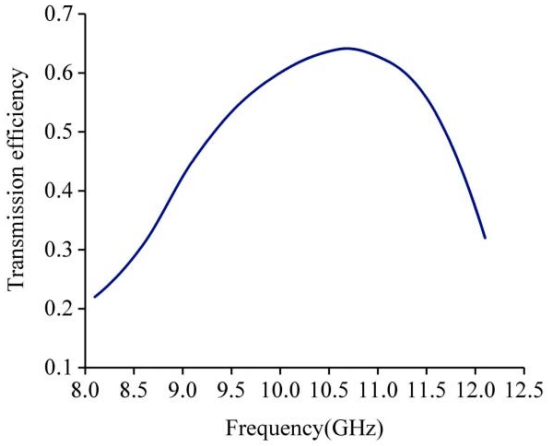

Fig. 6. Simulated transmission efficiency of OAM metalens.

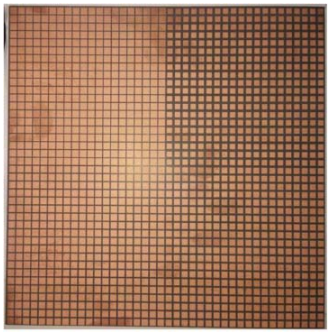

Fig. 7. Photograph of the fabricated metalens prototype that consists of eight zones.

Fig. 5(b) shows the intensity distribution on the same plane. Obviously, the helical phase changes from $-\pi$ to π, which is identical with OAM of $l = 1$. In addition, though there is a small gap on the right side of the ring-shaped intensity distribution due to the fact that the transmission coefficient of unit 1 and unit 8 are a little bit lower than that of the other unit cells, it still can be seen that there is a typical doughnut-shaped intensity with zero intensity in the center. Also, that is the reason why the intensity of the right part is smaller than that of the left side on the *xoz* plane ($y = 0$), as shown in Fig. 5(c). Overall, the simulation results of both phase and intensity distributions are in good agreement with the theoretical prediction, indicating that a vortex beam carrying the OAM mode with a topological charge of 1 is generated in the transmission.

In addition, as shown in Fig. 6, the transmission efficiency of the OAM metalens exceeds 60% from 10 to 11.3 GHz. It should be noticed that the high efficiency is calculated in terms of energy; however, it is lower than the prediction of 80% according to the transmission coefficient of the unit cell. This is mainly caused by the discrepancies in the transmission coefficients of the individual elements constituting the metalens, which may result in mutual influence when forming the vortex beam.

Then, the metalens prototypes are fabricated with an array of 1600 unit cells, and the total physical dimension is 240 mm × 240 mm, as shown in Fig. 7. All the parameters, including the geometric size of the metallic part and the

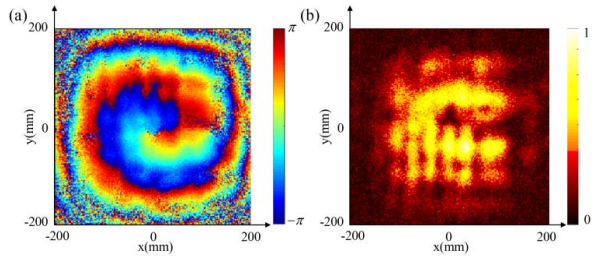

Fig. 8. Measurement results of the transmitted wave emitted from the metalens generating vortex beam carrying OAM mode of 1. (a) Phase distribution in the *xoy* plane ($z = 200$ mm). (b) Energy distribution in the same location.

relative permittivity of the dielectric substrate, are the same as that used in the simulations.

The metalens prototype is then measured in a microwave anechoic chamber. In order to obtain a uniform plane wave, the linearly polarized horn antenna is placed with a distance of 400 mm away from the metalens. A receiving probe is placed in the horizontal direction and the vertical direction, respectively, to measure the amplitude and phase of the transmitted wave, and the measured data are recorded and processed in the vector network analyzer (Agilent 8722 ES). Fig. 8 shows the phase and intensity distributions with a distance of 200 mm away from the metalens at 10.6 GHz. As can be seen, the phase of the transmitted wave has a distinct single helix gradient, varying from $-\pi$ to π. Moreover, the intensity map is similar to the circular ring distribution with a small gap and the intensity of the center approaches to 0. The measurement results show good agreements with the simulation results, which further verify the design approach.

V. Conclusion

In summary, a high-efficiency metalens working at X-band is presented based on MEFSS to generate vortex beam carrying OAM mode in this paper. A group of MEFSS unit cells is proposed as spatial phase shifters, and the whole metalens exhibits a high efficiency of over 60% in the operation band from 10 to 11.3 GHz. The measurement results are in good agreement with simulation results. Though there is a little defect in energy distribution that needs to be improved in the future work, this method provides a promising way to generate vortex beam carrying OAM modes at microwave region.

Acknowledgment

This work was supported by the National Natural Science Foundation of China under Grant 61 771 172, Grant 61 571 155, and Grant 61 401 122.

References

[1] L. Zhang, K. Zhang, J. Peng, J. Deng, Y. Yang, and J. Ma, "Circular photonic crystal fiber supporting 110 OAM modes," *Opt. Commun.*, vol. 429, pp. 189–193, Dec. 2018.

[2] J. Wang, "Twisted optical communications using orbital angular momentum," *Sci. China Phys., Mech. Astron.*, vol. 62, no. 3, p. 4201, Mar. 2019.

[3] L. Allen, M. W. Beijersbergen, R. J. C. Spreeuw, and J. P. Woerdman, "Orbital angular momentum of light and the transformation of Laguerre-Gaussian laser modes," *Phys. Rev. A, Gen. Phys.*, vol. 45, no. 11, pp. 8185–8189, Jun. 1992.

[4] B. Thidé *et al.*, "Utlilization of photon orbital angular momentum in the low-frequency radio domain," *Phys. Rev. Lett.*, vol. 99, no. 8, Aug. 2007, Art. no. 087701.

[5] C. Shi, M. Dubois, Y. Wang, and X. Zhang, "High-speed acoustic communication by multiplexing orbital angular momentum," *Proc. Nat. Acad. Sci. USA*, vol. 114, no. 28, pp. 7250–7253, 2017. doi: 10.1073/pnas.1704450114.

[6] M. A. Salem and C. Caloz, "Precision orbital angular momentum (OAM) multiplexing communication using a metasurface," in *Proc. Int. Congr. Adv. Electromagn. Mater. Microw. Optics*, Sep. 2013, pp. 94–96.

[7] Y. Yan *et al.*, "High-capacity millimetre-wave communications with orbital angular momentum multiplexing," *Nature Commun.*, vol. 5, p. 4876, Mar. 2014.

[8] S. M. Mohammadi *et al.*, "Orbital angular momentum in radio—A system study," *IEEE Trans. Antennas Propag.*, vol. 58, no. 2, pp. 565–572, Feb. 2010.

[9] J. Liang and S. Zhang, "Orbital angular momentum (OAM) generation by cylinder dielectric resonator antenna for future wireless communications," *IEEE Access*, vol. 4, pp. 9570–9574, 2016.

[10] X. Hui *et al.*, "Ultralow reflectivity spiral phase plate for generation of millimeter-wave OAM beam," *IEEE Antennas Wireless Propag. Lett.*, vol. 14, pp. 966–969, 2015.

[11] Z. Zhang, S. Xiao, Y. Li, and B.-Z. Wang, "A circularly polarized multimode patch antenna for the generation of multiple orbital angular momentum modes," *IEEE Antennas Wireless Propag. Lett.*, vol. 16, pp. 521–524, 2017. doi: 10.1109/LAWP.2016.2586975.

[12] Y. M. Zhang and J. L. Li, "Analyses and full-duplex applications of circularly polarized OAM arrays using sequentially rotated configuration," *IEEE Trans. Antennas. Propag.*, vol. 66, no. 12, pp. 7010–7020, Dec. 2018.

[13] A. S. Sebastian *et al.*, "Plasmonic metasurfaces for the generation of optical orbital angular momentum," *Current Opinion Colloid Interface Sci.*, vol. 19, no. 3, pp. 207–215, 2014.

[14] X. L. Chen, H. Zhou, M. Liu, and J. Dong, "Measurement of orbital angular momentum by self-interference using a plasmonic metasurface," *IEEE Photon. J.*, vol. 8, no. 1, Feb. 2016, Art. no. 4800308.

[15] Y. Meng, J. Yi, S. N. Burokur, L. Kang, H. Zhang, and D. H. Werner, "Phase-modulation based transmitarray convergence lens for vortex wave carrying orbital angular momentum," *Opt. Express*, vol. 26, no. 17, pp. 22019–22029, Aug. 2018.

[16] M. W. Beijersbergen, R. P. C. Coerwinkel, M. Kristensen, and J. P. Woerdman, "Helical-wavefront laser beams produced with a spiral phaseplate," *Opt. Commun.*, vol. 112, pp. 321–327, Dec. 1994.

[17] Y. Y. Yuan, K. Zhang, X. Ding, B. Ratni, S. N. Buroku, and Q. Wu, "Complementary transmissive ultra-thin meta-deflectors for broadband polarization-independent refractions in the microwave region," *Photon. Res.*, vol. 7, no. 1, pp. 80–88, Jan. 2019.

[18] M. Titaouine, A. G. Neto, H. Baudrand, and F. Djahli, "Analysis of frequency selective surface on isotropic/anisotropic layers using WCIP method," *ETRI J.*, vol. 29, no. 1, pp. 36–44, Feb. 2007.

[19] G. Q. Luo, W. Hong, Q. H. Lai, and L. L. Sun, "Multilayer frequency selective surface with grating lobe suppression," *Microw. Opt. Technol. Lett.*, vol. 49, no. 10, pp. 2501–2503, Oct. 2007.

[20] R. Pous and D. M. Pozar, "A frequency-selective surface using aperture-coupled microstrip patches," *IEEE Trans. Antennas Propag.*, vol. 39, no. 12, pp. 1763–1769, Dec. 1989.

[21] M. Al-Joumayly and N. Behdad, "A new technique for design of low-profile, second-order, bandpass frequency selective surfaces," *IEEE Trans. Antennas Propag.*, vol. 57, no. 2, pp. 452–459, Feb. 2009.

[22] S. M. A. M. H. Abadi and N. Behdad, "Inductively-coupled miniaturized-element frequency selective surfaces with narrowband, high-order bandpass responses," *IEEE Trans. Antennas Propag.*, vol. 63, no. 11, pp. 4766–4774, Nov. 2015.

[23] R. Rodriguez-Berral, F. Medina, F. Mesa, and M. Garcia-Vigueras, "Quasi-analytical modeling of transmission/reflection in strip/slit gratings loaded with dielectric slabs," *IEEE Trans. Microw. Theory Techn.*, vol. 60, no. 3, pp. 405–418, Mar. 2012.

[24] O. Luukkonen *et al.*, "Simple and accurate analytical model of planar grids and high-impedance surfaces comprising metal strips or patches," *IEEE Trans. Antennas Propag.*, vol. 56, no. 6, pp. 1624–1632, Jun. 2010.